V European Conference on Computational Fluid Dynamics
ECCOMAS CFD 2010
J. C. F. Pereira and A. Sequeira (Eds)
Lisbon, Portugal, 14–17 June 2010

SOMMERFELD RADIATION CONDITION FOR INCOMPRESSIBLE VISCOUS FLOWS

Takashi Yoshida[*]**, Takashi Watanabe**[†]

[*]Shinshu University
Department of Environmental Science and Technology, Faculty of Engineering
Wakasato 4-17-1, Nagano 380-8553, Japan
e-mail: yoshi-t@shinshu-u.ac.jp

[†]Nagoya University
Graduate School of Information and Science
Furo-cho Chikusa-ku, Nagoya, 464-8601, Japan
e-mail: takashi@is.nagoya-u.ac.jp

Key words: Incompressible flow, Finite difference method, Outflow boundary condition, Sommerfeld radiation condition, Convective velocity

Abstract. *This paper investigates the methods of determining the convective velocity of the Sommerfeld radiation condition for incompressible Navier-Stokes equations in primitive variables. The Sommerfeld radiation condition for incompressible flows is a one-dimensional convective equation and has been widely used for outflow boundary condition of spatial developing flows. The definition of its convective velocity is unclear and the selection of appropriate value for the convective velocity is a critical issue. Four decision methods of the convective velocity with finite difference method are considered: the mean velocity over the exit boundary, the arithmetic mean velocity of the maximum and the minimum velocities on the outflow boundary, the local instantaneous velocity, and the numerically evaluated convective velocity which is modified procedure of Orlanski's open boundary condition. These methods are applied to two test problems for comparison. The first case is two Lamb dipoles traveling in a slow uniform flow. The second case is a two-dimensional impulsively starting jet flow. The numerical evaluated convective velocity produces minimum distortion and deformation of a vortex and provides no reflection.*

1 INTRODUCTION

Many problems in fluid dynamics are defined in unbounded domains. These domains have to be truncated in order to compute flow fields in finite computational domains. The artificial boundary conditions are needed to be defined on the boundaries of truncated computational domain. The formulation of these boundary conditions, especially the outflow boundary conditions, is a very important and difficult issue. Although the flow field near the outflow boundary depends on the flow outside the computational domain, the velocity outside the domain is unknown and unavailable. The incompressible Navier-Stokes equations are elliptic, so that unsuitable outflow boundary conditions may influence the numerical solution in the whole domain and yield numerical instability. The problem of outflow boundary conditions for unsteady incompressible flow has been a matter of discussion and is still a subject of active studies. More details about the issue of outflow boundary conditions are found in review articles by Gresho[1, 2, 3] and Sani and Gresho[4].

One of the most successful outflow boundary conditions for numerical simulations of unsteady incompressible flows by the finite difference method is the Sommerfeld radiation condition, which is also called the convective boundary condition. The Sommerfeld radiation condition for incompressible flows is a one-dimensional convective equation and the convective velocity of this condition is an arbitrary value. It is defined as “a representative value” of the normal velocity at the exit (see Gresho[1, 2, 3]). The Sommerfeld radiation condition has been employed in many investigations and the convective velocity has been defined in different manners. Pauley et al.[5], Salvetti et al.[6], Verzicco et al.[7], Lim and Redekoppa[8] and Ruith et al.[9] reported that the value of convective velocity is not critical to the numerical solution. On the other hand, Hasan et al.[10] mentioned that the quantity of the convective velocity was loosely defined and was determined by trial and error in previous literatures. Ol’shanskii and Staroverov[11] also pointed out that the good choice of the convective velocity is quite important. Therefore, it is an open issue how to determine which value is appropriate for the convective velocity.

The main objective of this paper is to investigate the proper choice of the convective velocity for the Sommerfeld radiation condition. We select four methods of determining the convective velocity and apply them to two test cases for two-dimensional incompressible viscous flow, which are two Lamb dipoles traveling in a slow uniform flow and a two-dimensional impulsively starting jet flow. We will demonstrate the sensitivity of the results to the method of determining the convective velocity.

2 NUMERICAL METHOD AND BOUNDARY CONDITIONS

2.1 Numerical method

The governing equations are the Navier-Stokes equations and the equation of continuity in two-dimensional Cartesian coordinates for viscous incompressible flow,

$$\frac{\partial u}{\partial t} + u\frac{\partial u}{\partial x} + v\frac{\partial u}{\partial y} = -\frac{\partial p}{\partial x} + \frac{1}{Re}\left(\frac{\partial^2 u}{\partial x^2} + \frac{\partial^2 u}{\partial y^2}\right), \tag{1}$$

$$\frac{\partial v}{\partial t} + u\frac{\partial v}{\partial x} + v\frac{\partial v}{\partial y} = -\frac{\partial p}{\partial y} + \frac{1}{Re}\left(\frac{\partial^2 v}{\partial x^2} + \frac{\partial^2 v}{\partial y^2}\right), \tag{2}$$

$$\frac{\partial u}{\partial x} + \frac{\partial v}{\partial y} = 0\,. \tag{3}$$

These equations have been nondimentionalized using a characteristic velocity and a characteristic length. The spatial discretization of these equations is the finite difference method on a non-uniform staggered grid. The convective terms in the momentum equations are discretized with the fully conservative second order finite difference scheme of Morinishi et al.[12]. The remaining terms are discretized with second order central difference schemes. Time integration of governing equations is carried out using P2 pressure correction method, which is a kind of fractional step methods, proposed by Armfield and Street[13] with Kim and Moin boundary condition[14]. The second order Adams-Bashforth method is used for convective terms and the Crank-Nicolson method is used for viscous terms. The overall accuracy of this method is second order in time.

2.2 Outflow boundary conditions

We consider the Sommerfeld radiation condition for incompressible flows in two-dimensional Cartesian coordinates. These take the form

$$\frac{\partial u}{\partial t} + U_c \frac{\partial u}{\partial x} = 0 \ , \tag{4}$$

$$\frac{\partial v}{\partial t} + U_c \frac{\partial v}{\partial x} = 0 \ , \tag{5}$$

where x is the outflow direction and U_c is the convective velocity, which is a representative value of the normal velocity at the outflow boundary. These conditions are similar to Taylor's hypothesis of frozen flow. The value of U_c has been defined in different manners by different authors in many literatures. Therefore, a number of choices for U_c are possible. It is not clear which value of U_c is appropriate.

Equations (4) and (5) are discretized by a first order backward difference scheme in space on the staggered grid at the outflow boundary as shown in figure 1 and are integrated by explicit Euler method in time. The resulting finite difference forms are given as follows,

$$\frac{u^{n+1}_{IN+1/2,j} - u^{n}_{IN+1/2,j}}{\Delta t} + U_c \frac{u^{n}_{IN+1/2,j} - u^{n}_{IN-1/2,j}}{\Delta x_{IN}} = 0, \tag{6}$$

$$\frac{v^{n+1}_{IN+1,j+1/2} - v^{n}_{IN+1,j+1/2}}{\Delta t} + U_c \frac{v^{n}_{IN+1,j+1/2} - v^{n}_{IN-1,j+1/2}}{\Delta x_{IN+1/2}} = 0. \tag{7}$$

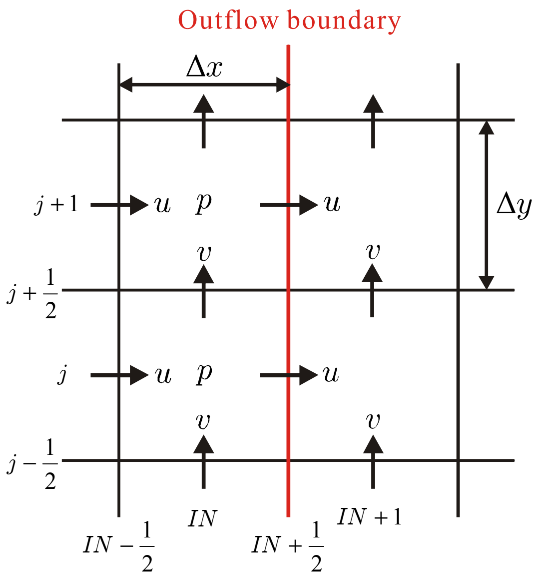

Figure 1: Staggered grid system near outflow boundary of computational domain.

The following four methods for determining the convective velocity are compared.

SRC1: The mean velocity over the outflow boundary.

$$U_c = \frac{Q_{\text{out}}}{H} = \frac{1}{H}\sum_j \left(u^n_{IN+1/2,j} \Delta y_j \right). \tag{8}$$

In this equation, Q_{out} is the outflow rate and H is the height of the outflow boundary. This condition has been used in Poiseuille-Bénard flow[15, 16, 17], plane turbulent wake[18], boundary layer separation[5], turbulent confined coannular jet[19], turbulent flow over a backward-facing step[20], and many others. Because U_c is constant and independent of y, normal velocity $u^{n+1}_{IN+1/2,j}$ calculated explicitly from equation (6) automatically satisfies the global mass conservation, i.e. the outflow rate equals the inflow rate at an each time step, as shown by Gresho[2]. No correction of $u^{n+1}_{IN+1/2,j}$ is necessary to guarantee the global mass conservation.

SRC2: The arithmetic mean velocity of the maximum and the minimum normal velocities at the outflow boundary.

$$U_c = \frac{\max\left(u^n_{IN+1/2,j}\right) + \min\left(u^n_{IN+1/2,j}\right)}{2}. \tag{9}$$

This method was proposed by Yoshida et al.[21] based the experimental investigation of the convective velocity of Taylor's hypothesis for large scale coherent structures in turbulent round jet by Zaman and Hussain[22]. They concluded that a single convection velocity should be used. But the structure convection velocity is generally neither unique nor easily measurable. They suggested to use the average of the velocities across the shear region, instead of the structure convection velocity. In numerical simulations, it is impossible to beforehand know the structure convection velocity and the shear region. Then we proposed to simply approximate the average velocity of shear region on the outflow boundary by the arithmetic mean of the maximum and minimum velocities.

SRC3: The local instantaneous velocity at previous time step.

$$U_c = u^n_{IN+1/2,j}. \tag{8}$$

This method has been employed by Nataf[23], Jin and Braza[24], and Hoarau et al.[25]. The value of U_c is local and dependent on y, so that the global mass conservation is not satisfied automatically. The outflow velocity $u^{n+1}_{IN+1/2,j}$ is corrected uniformly over the outflow boundary to ensure that the outflow rate Q_{out} balances the inflow rate Q_{in},

$$u^{n+1}_{IN+1/2,j} \leftarrow u^{n+1}_{IN+1/2,j} \times \frac{Q_{\text{in}}}{Q_{\text{out}}}. \tag{9}$$

SRC4: The numerically evaluated convective velocity. This method was originally designed by Orlanski for hyperbolic problems[26]. The convective velocity is calculated locally at the closest interior point and at the previous time level. Orlanski's original finite difference representation used a leapflog method. In this work, the original condition is modified using the explicit Euler method and the first order backward difference in the following way,

$$U_c = -\frac{\Delta x_{IN-1}}{\Delta t}\frac{u^{n}_{IN-1/2,j} - u^{n-1}_{IN-1/2,j}}{u^{n-1}_{IN-1/2,j} - u^{n-1}_{IN-3/2,j}}, \tag{10}$$

$$U_c = -\frac{\Delta x_{IN-1/2}}{\Delta t}\frac{v^{n}_{IN-1,j+1/2} - v^{n-1}_{IN-1,j+1/2}}{v^{n-1}_{IN-1,j+1/2} - v^{n-1}_{IN-2,j+1/2}}. \tag{11}$$

We apply the same constraint of the original Orlanski method to U_c, i.e.,

$$\begin{aligned} U_c &= 0, && \text{if } U_c \le 0, \\ U_c &= -\frac{\partial u/\partial t}{\partial u/\partial x}, && \text{if } 0<U_c<\frac{\Delta x_{IN-1}}{\Delta t}, \\ U_c &= \frac{\Delta x_{IN-1}}{\Delta t}, && \text{if } U_c \ge \frac{\Delta x_{IN-1}}{\Delta t}. \end{aligned} \tag{12}$$

The lower limit $U_c = 0$ does not allow information to come from outside to inside the computational domain. The upper limit $U_c = \Delta x_{IN-1}/\Delta t$ is due to the Courant-Friedrichs-Lewy condition for numerical stability. This method is similar to that used by Han et al.[27] for linear hyperbolic and parabolic problems. Although Orlanski proposed this condition for hyperbolic problem, we apply this method to incompressible fluid flows that have elliptic character. Because the convective velocity is calculated locally, the global mass conservation is not satisfied automatically. Then, the correction scheme prescribed by equation (9) is also employed for SRC4.

3 RESULTS

The four methods for determining the convective velocity of the Sommerfeld radiation condition are applied to two test cases. The first case is two Lamb dipoles traveling in a slow uniform flow. The second case is a two-dimensional impulsively starting jet flow.

3.1 Two Lamb dipoles traveling in a slow uniform flow

The Lamb dipole is the exact solution of Euler equations[28], assuming that vorticity ω is related to function ψ by $\omega = k^2\psi$ inside a circular region with radius R_c, while the exterior flow is irrotational. The stream function of the Lamb dipole in polar coordinates (r,θ) is

$$\psi(r,\theta) = \begin{cases} \dfrac{2U_L}{kJ_0(kR_c)} J_1(kr)\ \sin\theta, & (r \le R_c), \\ U_L\left(r - \dfrac{R_c^2}{r}\right)\sin\theta, & (r > R_c)\ . \end{cases} \tag{13}$$

The function J_0 and J_1 are the zeroth- and first-order Bessel functions of the first kind, respectively. U_L is the propagation velocity of the dipole in a inviscid fluid. The value of k is determined by the first zero point of $J_1(x)$,

$$J_1(kR_c) = 0, \quad kR_c \approx 3.8317. \tag{14}$$

The dipole is superimposed on a slow uniform flow. The velocity of the uniform flow is 0.1, and the propagation velocity of the dipole is $U_L = 0.9$. Then the initial traveling velocity of the dipole is $U = 1.0$. The radius of dipole is $R_c = 1.0$ and the Reynolds number is $Re = UR_c/\nu = 500$.

The computational domains and the boundary conditions are shown in figure 2. Computations are performed with two different domain sizes. One is a short domain and the other is a long domain corresponding to $x = 10$ and $x = 15$, respectively. We refer to the solution of the long domain as "exact", because the outflow boundary is located far downstream. The grid space is uniform in x direction with 1250 points for the short domain and 1875 points for the long domain. The grid points in y direction are 700 and uniform in $-3 \le y \le +3$. Two Lamb dipoles are located in series and centered at (2.5, 0.0) and (4.0, 0.0). Figure 3 shows the initial vorticity field, where red color contours represent positive values and blue color contours represent negative values of vorticity.

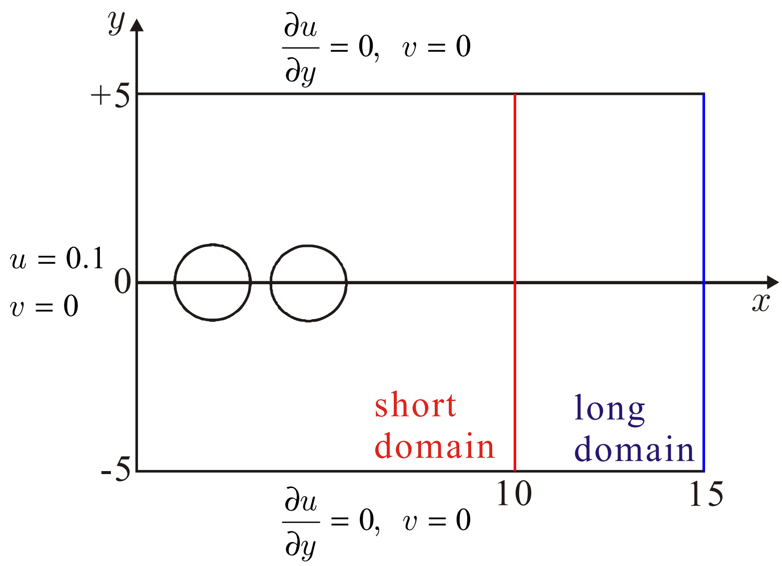

Figure 2: Computational domains and boundary conditions for the two Lamb dipoles convecting flow.

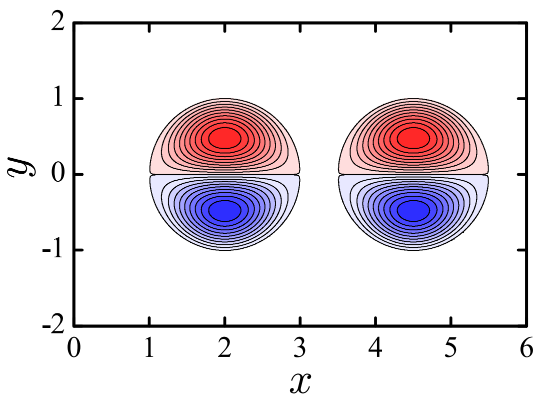

Figure 3: Contours of vorticity of the initial dipoles. Red color contours represent positive vorticity, and Blue color contours represent negative vorticity.

Calculations by the four SRC methods were performed in both short and long domains with the time step $\Delta t = 0.01$. Figure 4 shows instantaneous vorticity field at $t = 6$ with the different SRCs in the short domain and in the long domain. In figure 4(a),

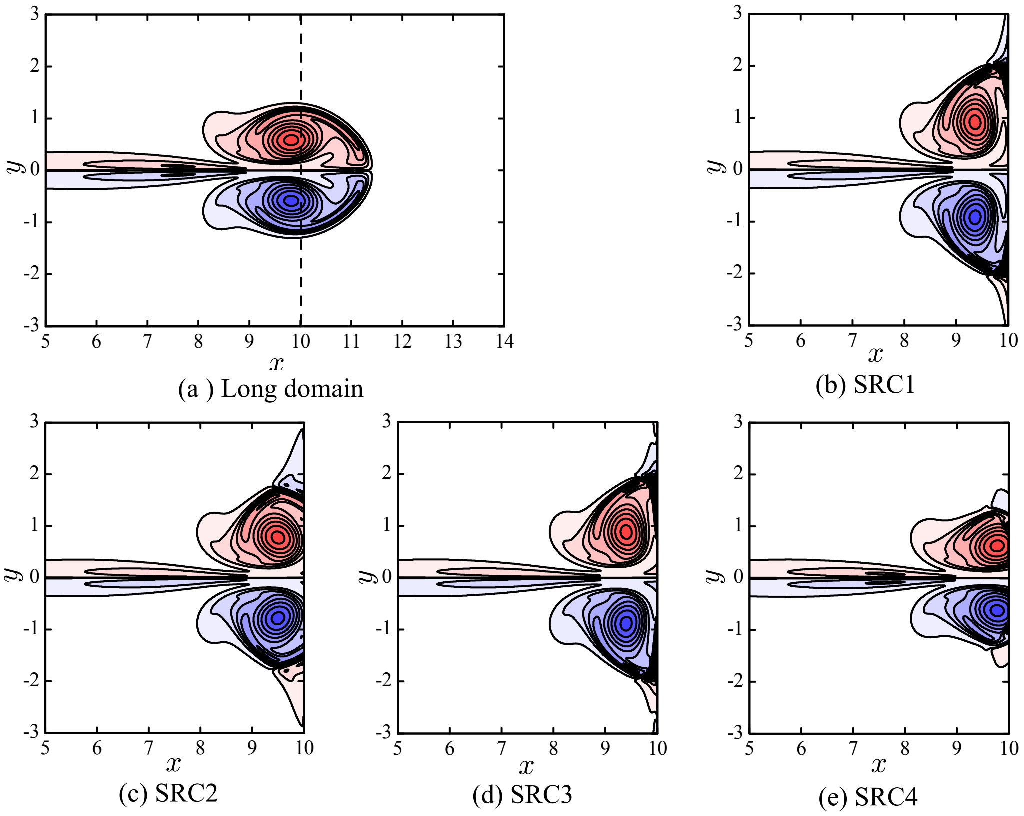

Figure 4: Vorticity contures of the two Lamb dipoles at $t = 6$ for different SRCs.

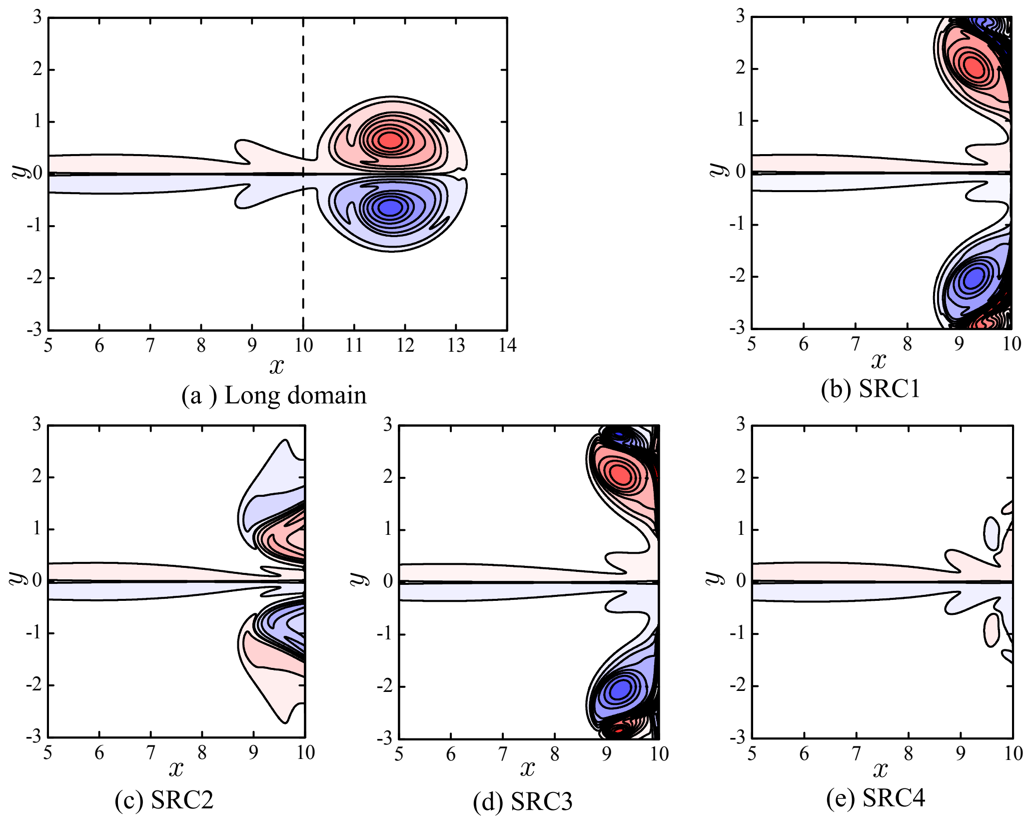

Figure 5: Vorticity contures of the two Lamb dipoles at $t = 8$ for different SRCs.

two Lamb dipoles merge into one dipole and the center of dipole passes through the section at $x = 10$ in the long domain. In the short domain, figure 4(b) - (e), the merged dipole approaches the outflow boundary. The dipole with SRC1 distorts and stretches in the tangential direction of outflow boundary as shown figure 4(b). Figure 4(c) and 4(d) show similar distortion of the vortex. In contrast, the vortex with SRC4 in figure 4(e) moves straight downstream with little distortion. Figure 5 shows vorticity filed at $t = 8$. In the long domain as shown figure 5(a), the merged dipole has already passed over the line at $x = 10$. For SRC1 and SRC3, the dipole rebounds at the outflow boundary and induces secondary vortices outside of the main vortices, that have strong opposite sign vorticity shown in figure 5(b) and 5(d). This behavior of the dipole is similar to the result of numerical simulation for the vortex dipole rebound from a nonslip wall by Orlandi[29]. Figure 5(c) shows deformation of the vortex, although there is no strong reflection of vorticity. Figure 5(e) shows the vorticity field obtained by using SRC4. The distribution of vorticity in figure 5(e) is almost agree with that of corresponding region in the long domain shown in figure 5(a). This demonstrates that SRC4 provides a smooth passage of vortex structure and gives no reflection of vorticity.

3.2 Two-dimensional impulsively starting jet flow

The second test problem is a two-dimensional impulsively starting jet flow. The computational domains and boundary conditions are shown in figure 6. The width of nozzle is the characteristic length. An inlet flow at the entrance of the nozzle is discharged impulsively into a quiescent fluid. A uniform velocity profile is imposed at the inlet. The Reynolds number based on the nozzle width and the uniform velocity is 100. The impulsively discharged flow from the nozzle forms a vortex dipole in the front region of the jet.

Two computational domains are also used in this test. One is the short domain and the other is long domain. The length of nozzle is 0.5 in both domains. The short domain is $-0.5 \le x \le 6$ and $-8 \le y \le 8$ with 650×420 mesh. The long domain is $-0.5 \le x \le 12$ and $-8 \le y \le 8$ with 1250×420 mesh. The grid space in x direction is

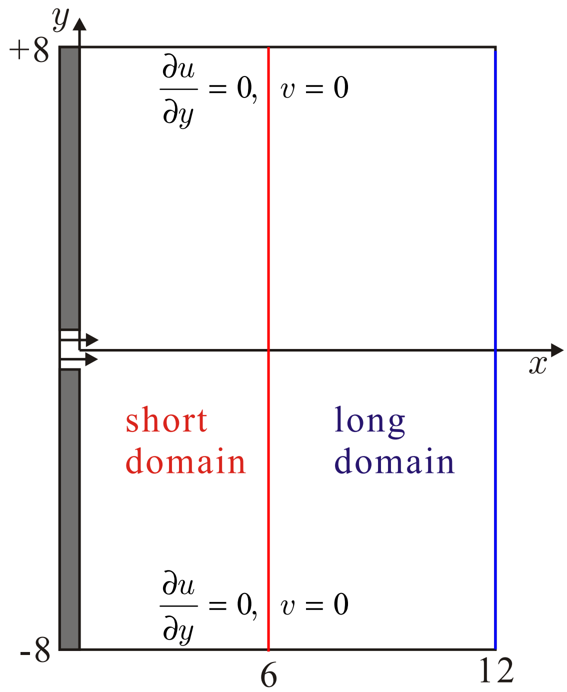

Figure 6: Computational domains and boundary conditions for the two dimensional impulsively jet flow.

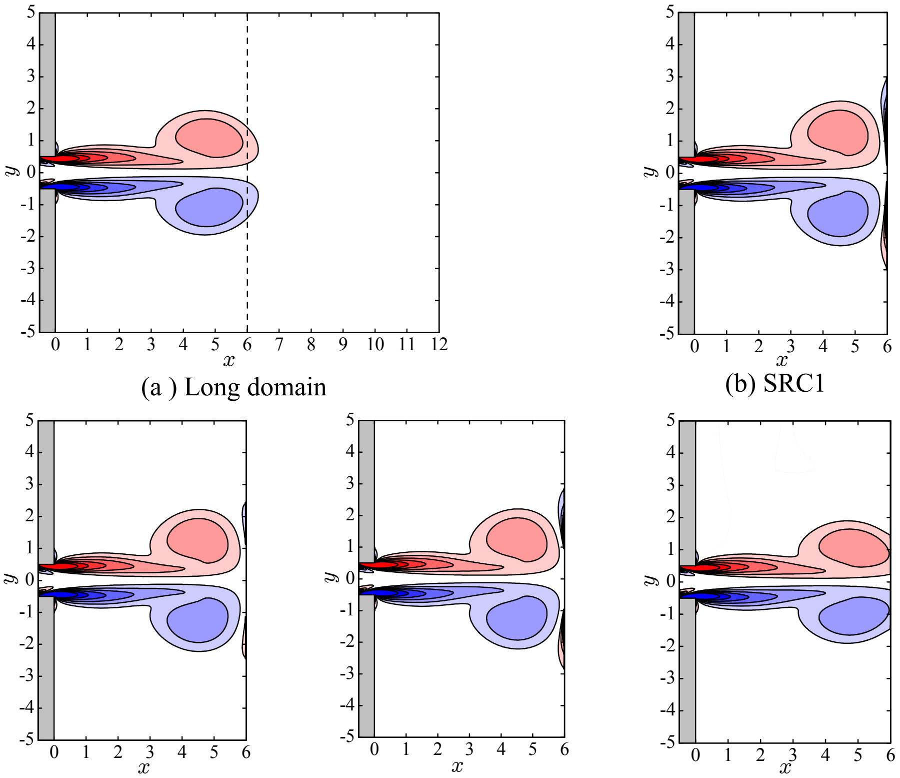

(a) Long domain (b) SRC1

(c) SRC2 (d) SRC3 (e) SRC4

Figure 7: Vorticity contures of the two-dimensional jet at t = 15 for different SRCs.

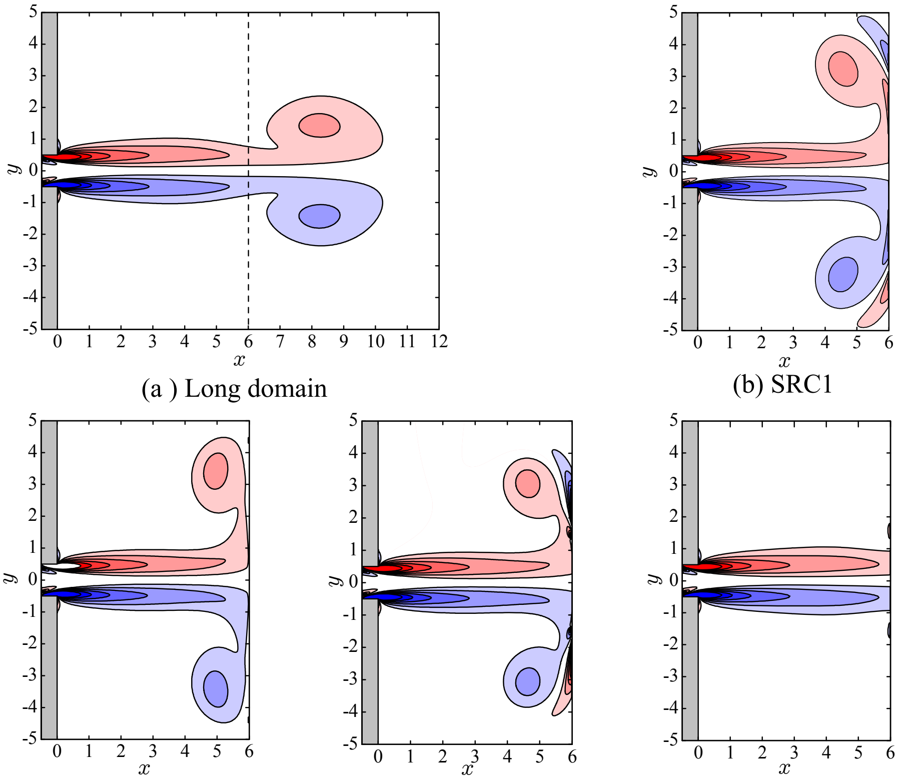

(a) Long domain (b) SRC1

(c) SRC2 (d) SRC3 (e) SRC4

Figure 8: Vorticity contures of the two-dimensional jet at t = 25 for different SRCs.

uniform and is nonuniform in y direction.

Figure 7 shows instantaneous vorticity field at $t = 15$ with the different SRCs in the short domain and in the long domain. As indicated in figure 7(a), a vortex dipole is formed at the front of jet through roll up of the jet shear layer and moves downstream. The front of the dipole passes through the cross section at $x = 6$ in the long domain. The dipole of SRC1 is slightly expanded in transverse direction and induces vorticity sheets at the outflow boundary. The behaviors of SRC2 and SRC3 are almost similar to SRC1. The vorticity distribution obtained with SRC4 in figure 7(e) is in good agreement with that of long domain.

Figure 8 shows instantaneous vorticity field at $t = 25$. For SRC1, SRC2, and SRC3, the dipole rebounds from the outflow boundary. Then the dipole splits two monopole vortices and each vortex travels along the outflow boundary. On the other hand, the result by SRC4 in figure 8(e) shows no reflection of vorticity. The dipole has smoothly passed through the outflow boundary and the trailing jet has been remained in the short domain. The vorticity distribution is quite similar to that in the corresponding region of long domain as shown figure 8(a).

4 CONCLUSIONS

The outflow boundary condition for the incompressible Navier-Stokes equations is studied. The Sommerfeld radiation condition is employed for calculations using the finite difference method. The four different methods of determining its convective velocity are compared in two test cases, which are two Lamb dipoles traveling in a slow uniform flow and a two-dimensional impulsively starting jet flow. It is shown that the value of the convective velocity is critical to the solution in the interior domain. For the both test cases, the results of the numerically evaluated convective velocity (SRC4) show that the passage of the vortex dipole is very smooth and very good agreement with that of long domain. On the other hand, the other three methods yield large distortion of vertical structure and reflection from the outflow boundary.

REFERENCES

[1] P. M. Gresho, Incompressible fluid-dynamics - some fundamental formulation issues, *Annu. Rev. Fluid Mech.* **23**, 413-453 (1991).

[2] P. M. Gresho, Some interesting issues in incompressible fluid-dynamics, both in the continuum and in numerical-simulation, *Adv. Appl. Mech.* **28**, 45-140 (1991).

[3] P. M. Gresho, Some current CFD issues relevant to the incompressible Navier-Stokes equations, *Comp. Meth. Appl. Mech. Eng.* **87**, 201-252 (1991).

[4] R. L. Sani and P. M. Gresho, Résumé and remarks on the open boundary-condition minisymposium, *Int. J. Numer. Meth. Fluids* **18**, 983-1008 (1994).

[5] L. L. Pauley, P. Moin and W. C. Reynolds, The structure of two-dimensional separation, *J. Fluid Mech.* **220**, 397-411 (1990).

[6] M. V. Salvetti, P. Orlandi and R. Verzicco, Numerical simulations of transitional axisymmetric coaxial jets, *AIAA J.* **34**, 736-743 (1996).

[7] R. Verzicco, P. Orlandi, A. H. M. Eisenga, G. J. F. V. Heijst and G. F. Carnevale, Dynamics of a vortex ring in a rotating fluid, *J. Fluid Mech.* **317**, 215-239 (1996).

[8] D. W. Lim and L. G. Redekopp, Aerodynamic flow-vectoring of a planar jet in a co-flowing stream, *J. Fluid Mech.* **450**, 343-375 (2002).

[9] M. R. Ruith, P. Chen and E. Meiburg, Development of boundary conditions for direct numerical simulations of three-dimensional vortex breakdown phenomena in semi-infinite domains, *Comput. Fluids* **33**, 1225-1250 (2004).
[10] N. Hasan, S. F. Anwer and S. Sanghi, On the outflow boundary condition for external incompressible flows: A new approach, *J. Comput. Phys.* **206**, 661-683 (2005).
[11] M. A. Ol'shanskii and V. M. Staroverov, On simulation of outflow boundary conditions in finite difference calculations for incompressible fluid, *Int. J. Numer. Meth. Fluids* **33**, 499-534 (2000).
[12] Y. Morinishi, O. V. Vasilyev and T. Ogi, Fully conservative finite difference scheme in cylindrical coordinates for incompressible flow simulations, *J. Comput. Phys*. **197**, 686-710 (2004).
[13] S. Armfield and R. Street, An analysis and comparison of the time accuracy of fractional-step methods for the Navier-Stokes equations on staggered grids, *Int. J. Numer. Meth. Fluids* **38**, 255-282 (2002).
[14] J. Kim and P. Moin, Application of a fractional-step method to incompressible Navier-Stokes equations, *J. Comput. Phys*. **59**, 308-323 (1985).
[15] A. Bottaro, Note on open boundary-conditions for elliptic flows, *Numer. Heat Tranf. B-Fundam*. **18**, 243-256 (1990).
[16] M. H. Kobayashi, J. C. F. Pereira and J. M. M. Sousa, Comparison of several open boundary numerical treatments for laminar recirculating-flows, *Int. J. Numer. Meth. Fluids* **16**, 403-419 (1993).
[17] X. Nicolas, P. Traore, A. Mojtabi and J. P. Caltagirone, Augmented Lagrangian method and open boundary conditions in 2D simulation of Poiseuille-Benard channel flow, *Int. J. Numer. Meth. Fluids* **25**, 265-283 (1997).
[18] P. R. Voke and S. G. Potamitis, Numerical-simulation of a low-Reynolds-number turbulent wake behind a flat-plate, *Int. J. Numer. Meth. Fluids* **19**, 377-393 (1994).
[19] K. Akselvoll and P. Moin, Large-eddy simulation of turbulent confined coannular jets, *J. Fluid Mech*. **315**, 387-411 (1996).
[20] H. Le, P. Moin and J. Kim, Direct numerical simulation of turbulent flow over a backward-facing step, *J. Fluid Mech*. **330**, 349-374 (1997).
[21] T. Yoshida, T. Watanabe and I. Nakamura, Numerical study of outflow boundary conditions for time-dependent incompressible flows, *Trans. Japan Soc. Mech. Eng*. **61**-588, 2887-2895(1995), in Japanese.
[22] K. B. M. Q. Zaman and A. K. M. F. Hussain, Taylor hypothesis and large-scale coherent structures, *J. Fluid Mech*. **112**, 379-396 (1981).
[23] F. Nataf, An open boundary condition for the computation of the steady incompressible Navier-Stokes equations, *J. Comput. Phys*. **85**, 104-129 (1989).
[24] G. Jin and M. Braza, A nonreflecting outlet boundary condition for incompressible unsteady Navier-Stokes calculations," *J. Comput. Phys*. **107**, 239-253 (1993).
[25] Y. Hoarau, M. Braza, Y. Ventikos and D. Faghani, First stages of the transition to turbulence and control in the incompressible detached flow around a NACA0012 wing, *Int. J. Heat Fluid Flow* **27**, 878-886 (2006).
[26] I. Orlanski, A simple boundary condition for unbounded hyperbolic flows, *J. Comput. Phys*. **21**, 251-269 (1976).
[27] T. Y. Han, J. C. S. Meng and G. E. Innis, An open boundary condition for incompressible stratified flows, *J. Comput. Phys*. **49**, 276-297 (1983).
[28] H. Lamb, Hydrodynamics, 6th Edition, *Camblidge University Press* (1994).
[29] P. Orlandi, Vortex dipole rebound from a wall, *Phys. Fluids A*, **2**, 1429-1436 (1990).